Available online at www.sciencedirect.com

ScienceDirect

Procedia Structural Integrity 59 (2024) 538–544

Structural Integrity Procedia

www.elsevier.com/locate/procedia

VII International Conference "In-service Damage of Materials: Diagnostics and Prediction" (DMDP 2023)

Theoretical analysis of the microrelief of typical machine-made surfaces by SEM photogrammetry

Anna Uhl[a], Oleksandr Melnyk[a], Yuliia Melnyk[b], Oleg Vereshko[b], Inna Boyarska[b], Sviatoslav Homon[c], Leonid Kulakovskyi[d*]

[a] *Lesya Ukrainka Volyn National University, Lutsk, Ukraine, pr. Voli 13, 43000 Lutsk, Ukraine*
[b] *Lutsk National Technical University, Lvivska 75, 43018 Lutsk, Ukraine*
[c] *National University of Water and Environmental Engineering, Soborna 11, 33000 Rivne, Ukraine*
[d] *National Technical University of Ukraine "Igor Sikorsky Kyiv Polytechnic Institute", 03056 Peremogy Avenue 37, Kyiv, Ukraine*

Abstract

The article analyzes digital elevation models (DEMs) of typical mechanically formed surfaces. The theoretical issues of 3D modeling of typical "ideal" surfaces obtained, for example, by artificially growing single crystals, forming regular microrelief of materials, etc. are considered. For this purpose, the most typical stepped, spherical, cylindrical, and cubic machined microrelief surfaces were selected. The algorithms for analytical photogrammetric and digital processing of SEM stereo images are presented and illustrated by relevant examples. The results of numerical integration for different surfaces are consistent with a typical "stepped" surface.

© 2024 The Authors. Published by Elsevier B.V.
This is an open access article under the CC BY-NC-ND license (https://creativecommons.org/licenses/by-nc-nd/4.0)
Peer-review under responsibility of DMDP 2023 Organizers

Keywords: microrelief, surface, photogrammetry, electron microscope, single crystals.

* Corresponding author. Tel.: +38094536546.
E-mail address: kulakovskiyl@ukr.net

2452-3216 © 2024 The Authors. Published by ELSEVIER B.V.
This is an open access article under the CC BY-NC-ND license (https://creativecommons.org/licenses/by-nc-nd/4.0)
Peer-review under responsibility of DMDP 2023 Organizers
10.1016/j.prostr.2024.04.076

1. Introduction

Scanning electron microscopes (SEMs) are widely used today to study the microgeometry of surfaces, but obtaining quantitative information about microrelief with characteristic dimensions of the micron and submicron range faces serious difficulties, and in most cases, such studies are conducted monocularly, limited to the qualitative side of research. When the studied micro-object consists of elements of simple geometric shape (polyhedra, planes, spheres, etc.), this method allows the researcher to form a certain idea of the spatial structure of the micro-object. If the object under study is complex and its spatial structure is not known in advance, then it is simply impossible to correctly understand the spatial organization of the microstructure based on monocular observations alone. Therefore, there is a need to implement methods that would allow for three-dimensional restoration (reconstruction) of micro-objects.

Nomenclature

$\bar{K}_P$ - average roughness index
$\bar{K}_A$ - roughness index of individual areas
θ - orientation angle
r - radius

Today, many fields of science and technology (materials science, biology, medicine, etc.) use scanning electron microscopy with great success, which allows for the study (evaluation) of surface microreliefs, their features and characteristics at the micron and submicron levels. A microrelief is a three-dimensional object with a certain spatial organization and microstructure. At the same time, the microstructure can be considered as the result of spatial correlation in the location of individual irregularities, as it is deterministic or random, isotropic or anisotropic. For this reason, a complete description of the digital elevation model as a physical field involves the analytical interpretation of the digital elevation model (DEM) to obtain the joint distribution function z(x,y) and its first and second derivatives for any finite set of points.

To obtain these distributions, a significant amount of computation is required, so most of the works known to us (Lakshmi et al. (2020); Macek et al. (2021); Nichols and Lange, (2006)) use one-dimensional distribution laws when analyzing random fields. The construction or reconstruction of a digital microrelief model is the task of reconstructing a three-dimensional object from a 2-D SEM image, which (Scherrer et al. (2008)) considered to be an incorrect task, accompanied by certain difficulties in its implementation. The study of the microtopography of the surfaces of various materials using scanning electron microscopy is described in the following works (Yasniy et al., 2011; Uhl et al., 2020; Pukas et al., 2020; Uhl et al, 2021).

2. Methods of experimental research

Let's consider some theoretical issues of 3D modeling of typical "ideal" surfaces obtained, for example, by artificially growing single crystals, forming regular microrelief of materials, etc. As an example, let's consider the most typical machined microrelief surfaces: stepped, spherical, cubic, and cylindrical.

Let us consider a stepped surface as a typical example of a fracture surface. To evaluate how the results of DEM construction of stepped surfaces correspond to the study of arbitrary fracture surfaces in general, we use the theorem known in fracture surface profiling that "fracture surfaces with the same roughness indicators have approximately the same average roughness profiles" (Abe and Deckert (2021)). For an "ideal" (Fig. 1) stepped fracture surface, a general relationship between the average roughness profile (1) and the corresponding roughness of individual sections ($\bar{K}_A$) was obtained in:

$$\frac{1}{\overline{K_p}} = \frac{4}{\pi}\left[\frac{1}{K_A} - \frac{(2-K_A)}{3K_A^2} + \frac{(2-K_A)^2}{5K_A^2} - \frac{(2-K_A)^2}{7K_A^4} + \ldots\right]. \tag{1}$$

Writing the equation (1) in the form of a finite series, then after some transformations we get:

$$\frac{1}{\overline{K}_P} = \frac{4}{\pi}\sum_{n=0}^{\infty}\frac{(-1)^n(2-K_A)^n}{(2n+1)K_A^{n+1}}. \tag{2}$$

Analyzing the resulting expression, we can determine that when $\overline{K}_A = 2$ corresponding to a surface with an arbitrary curvature, the distribution of orientation of surface elements and the local curvature of individual sections of the fracture surface does not affect the unambiguousness of the correlation between $\overline{K}_A$ i $\overline{K}_P$. This result can be interpreted as follows: if we consider the first term in equation (2) to take into account the chaotic surface topography, then the higher-order terms can be considered as corrections for the deviation of the analyzed surface from a completely arbitrary fracture surface. It should be noted that when $\overline{K}_A = 1$, which corresponds to the case of "ideal flat fracture surface", then $\overline{K}_P = 2$.

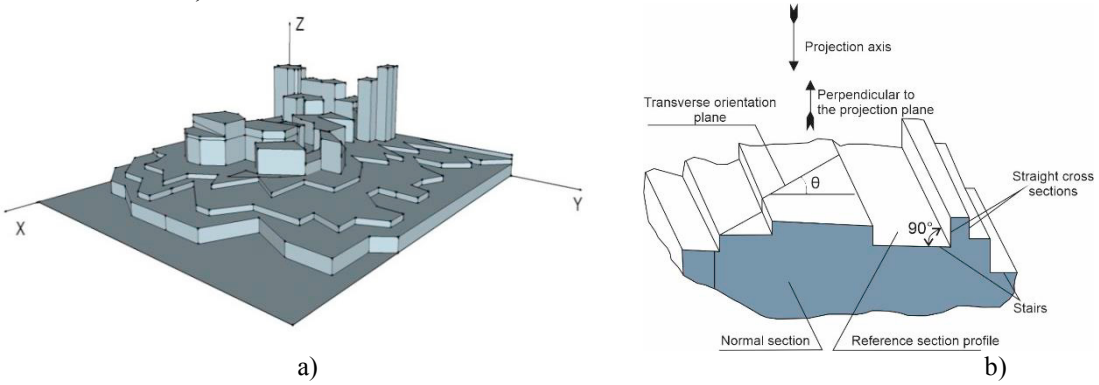

a) b)

Fig. 1. a) microrelief of the stepped plate type; b) "ideal" 3D stepped fracture surface of brittle fracture

When designing a hemispherical "ideal" surface on a base, the roughness index $\overline{K}_A$ for any normal section ABCE will be $\overline{K}_A = 2$, (Fig. 2). Then,

$$\overline{K}_P(\theta) = \frac{ABC(\theta)}{AEC(\theta)} = \frac{\pi r\sin\theta}{2r\sin\theta} = \frac{\pi}{2}. \tag{3}$$

and in the case of orientations of the sectional surface within $0 \le \theta \le \pi/2$ the average integral value is equal to

$\overline{K}_p = \int_0^{\pi/2} K_p(\theta)\rho(\theta)d\theta$. If, $\rho(\theta)d\theta = \frac{d\theta}{(\pi/2)}$, then for a hemisphere $\overline{K}_P = \pi/2$.

Comparing the relationship betw/een the average roughness profile and the corresponding roughness index of the section for the "ideal" stepped surface from equation (1) and the corresponding values of $\overline{K}_A$ i $\overline{K}_P$ for a hemispherical surface, it can be argued that fracture surfaces with arbitrary curvature and stepped surfaces are statically equivalent at the global level. However, they may be quite different "locally" (Yasniy et al., 2011).

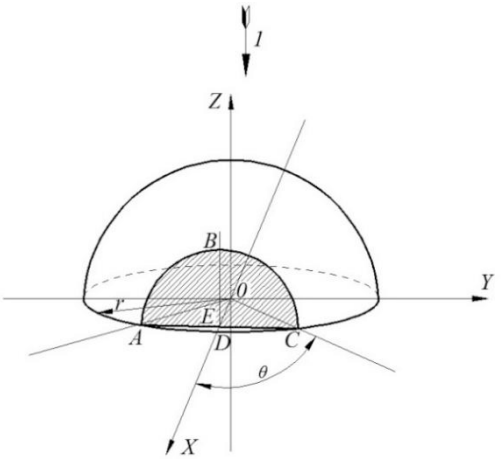

Fig. 2. A spherical fracture surface, where 1 is the projection axis with a parallel beam.

For semi-cylindrical surfaces:

$$\overline{K}_A = \frac{\pi rl}{2rl} = \frac{\pi}{2}. \tag{4}$$

For a normal section, unlike a spherical surface where parallel movement would be sufficient, we must randomize with respect to the orientation angle θ (Fig. 3). From this it follows that

$$\overline{K}_P(\theta) = \frac{ABC(\theta)}{AEC(\theta)}. \tag{5}$$

By averaging over all sections $0 \le \theta \le \pi/2$ and using $\rho(\theta)d\theta = \frac{2}{\pi}d\theta$, we get:

$$\overline{K}_P = \frac{2}{\pi}\int_0^{\pi/2}\int_0^{\pi/2}\sqrt{1-\sin^2\theta\sin^2\psi}\,d\theta d\psi\,. \tag{6}$$

This is a double elliptic integral of the second type, which can be calculated either digitally or by decomposing the internal integral into infinite series and integrating and substituting it into equation (7) to obtain the following expression:

$$\int_0^{\pi/2}\sqrt{1-\sin^2\theta\sin^2\psi}\,d\psi = \frac{\pi}{2}\left\{1-\left(\frac{1}{2}\right)^2\sin^2\theta-\left(\frac{1\cdot 3}{2\cdot 4}\right)^2\frac{\sin^4\theta}{3}-\left(\frac{1\cdot 3\cdot 5}{2\cdot 4\cdot 6}\right)^2\frac{\sin^6\theta}{5}-\ldots\right\}. \tag{7}$$

The integral in equation (6) converges rather quickly and gives $\overline{K}_P = 1.33725$.

To compare with a stepped surface, we substitute the values $\overline{K}_A$ from Equation (4) into Equation (2), and we get the value $\overline{K}_P = 1.33874$. This differs by about 0.1%.

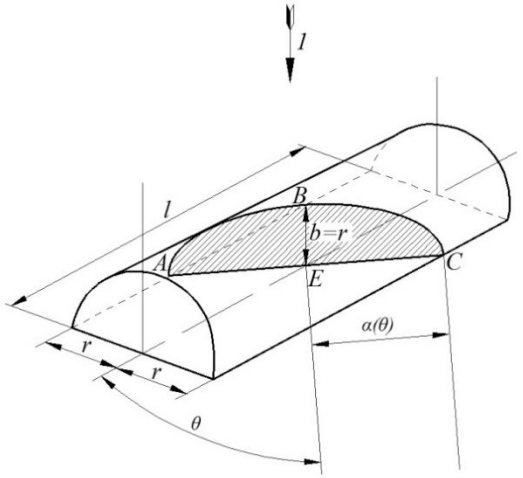

Fig. 3. Profilometric analysis of a circular semi-cylinder, where 1 is the projection axis with a parallel beam.

Let's consider another geometrically correct digital model of a microrelief obtained from a set of cubes of different sizes (Fig. 4). According to (Fig. 4, b), we will consider only the side and top surfaces of the cube, which are projected onto its base (so that =5 and can be determined from equation (7)).

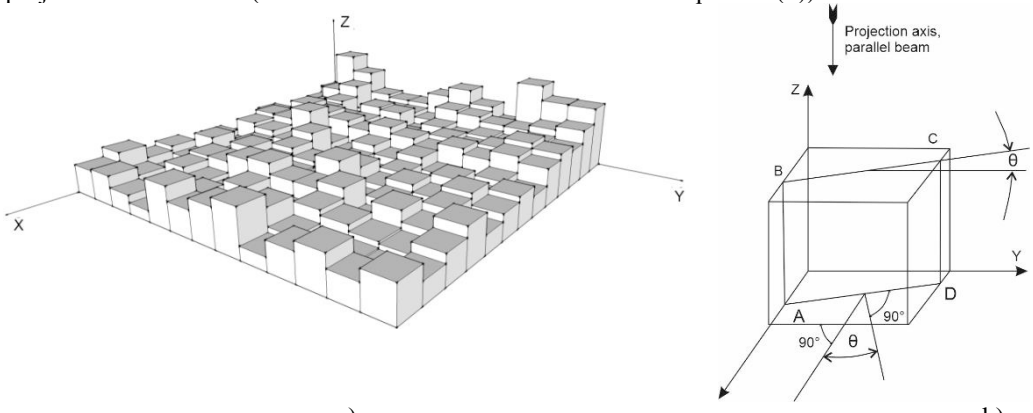

Fig. 4. Profilometric analysis of the cube: a) a geometrically correct microrelief model obtained from a set of cubes with different sizes; b) a scheme for analyzing the side and top surfaces of a cube that are projected onto its base.

For an arbitrary section perpendicular to the base $K_P(\theta) = ABCD / AD$, and for averaging over different orientations, it can be easily determined that

$$K_P(\theta) = \begin{cases} 1 + 2\cos\theta & for \quad 0 < \theta < \frac{\pi}{4} \\ 1 + 2\sin\theta & for \quad \frac{\pi}{4} < \theta < \frac{\pi}{2}. \end{cases} \tag{8}$$

Considering that $p(\theta)d\theta = d\theta/(\pi/2)$, get

$$\overline{K}_P = \frac{2}{\pi}\left\{\int_0^{\pi/4}(1+2\cos\theta)d\theta + \int_{\pi/4}^{\pi/4}(1+2\sin\theta)d\theta\right\}. \quad (9)$$

and $\overline{K}_P$=2,80063.

For the harmonic mean, we get $\overline{K}_P$=2,79907, which is practically the same. For parallel lines, it can be easily noted that $\overline{K}_P$=3, while for octahedral-type lines it is $\overline{K}_P$=2,78. Noting that in this case K_A=5, we obtain the corresponding value of $\overline{K}_P$, which is provided by equation (8) (for a stepped fracture surface).

3. Research results and discussion

A comparison of the projected areas and projected profiles of the above surfaces during theoretical calibration is shown in Table 1.

Table 1: Comparison of the projected area and projected profile of different surfaces during theoretical calibration.

Surface	$\overline{K}_A$	$\overline{K}_P$	$\overline{\overline{K}}_P$ by eq. 2	% dev. from eq. 2	Average % error for all surfaces
Stepped	1;2	18	18	0	2% for the arithmetic mean 3% for the harmonic mean
Spherical	2	π/2	π/2	0	
Cylindrical	π/2	1.33725	1.33874	0.111	
Cubic	5	2.79907	2.80063	0.066	

The results of numerical integration for different surfaces are consistent with a typical "stepped" surface. To correctly determine the values of $\overline{K}_A$ and $\overline{K}_P$, which are important for fractography, the differences should be 2-3%, which is practically insignificant.

Fig. 5, Fig. 6, Fig. 7, Fig. 8 shows the results of the practical application of digital stereometric processing of the SEM stereo image of a cast iron plate fracture sample.

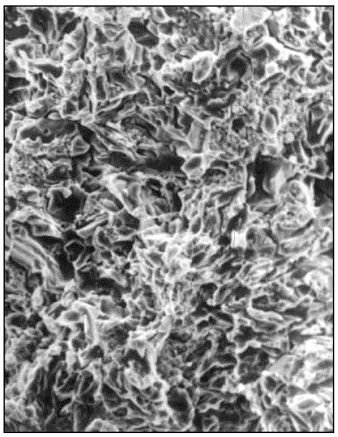

Fig. 5. SEM micrograph of the cast iron sample. Magnification 1000×.

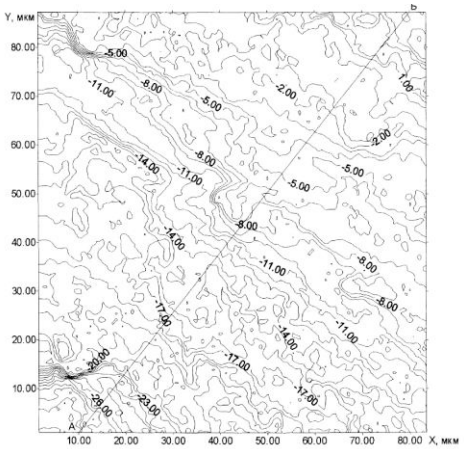

Fig. 6. Map of isolines of the fracture surface microrelief. Magnification 1000×.

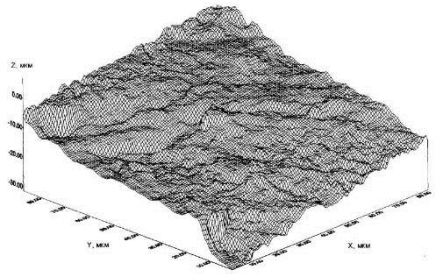

Fig. 7. 3D reconstruction of the fracture surface area. Magnification 1000×.

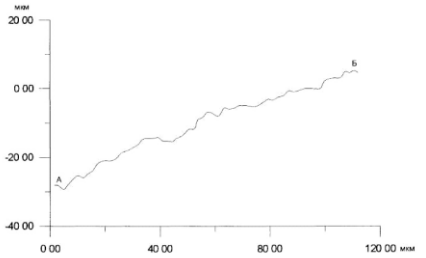

Fig. 8. Microrelief profile along the A-B line. Magnification 1000×.

4. Conclusions

Quantitative scanning electron microscopy methods can be successfully applied to the realization of tasks for which quantitative analysis of images of fine structure or surface relief using stereo measurements is most appropriate and, in some cases, dominant.

Methods of digital surface models of microobjects can be the basis for photogrammetric support of three-dimensional reconstruction of electron microscopic images.

References

Abe, S., Deckert, H., 2021. Roughness of fracture surfaces in numerical models and laboratory experiments. Solid Earth 12(10), 2407–2424.

Lakshmi, A. A., Rao, C. S., Buddi, T., 2020. Fractography analysis and constitutive modeling for dynamic plasticity of austenite stainless steel (ASS 304) at hot-working temperatures. Modern Manufacturing Processes 97-129.

Macek, W., Marciniak, Z., Branco, R., Rozumek, D., Królczyk, G. M., 2021. A fractographic study exploring the fracture surface topography of S355J2 steel after pseudo-random bending-torsion fatigue tests. Measurement 178, 109443.

Nichols, A. B., Lange, D. A., 2006. 3D surface image analysis for fracture modeling of cement-based materials. Cement and Concrete Research 36(6), 1098–1107.

Pukas, S., Zinko, L., German, N., Gladyshevskii, R., Koval, I.V., Bodrova, L., Kramar, H., Marynenko, S., 2020. Influence of the nano-WC content and Sintering Temperature on the Phase Composition of Hard Alloys in the System TiC–WC–VC–NiCr. Physics and Chemistry of Solid State 21(3), 496-502.

Scherrer, S. S., Quinn, G. D., Quinn, J. B., 2008. Fractographic failure analysis of a Procera® AllCeram crown using stereo and scanning electron microscopy. *Dental Materials* 24(8), 1107–1113.

Uhl, A., Melnyk, Y., Melnyk, O., Boyarska, I., Melnychuk, M., 2020. Application of Microphotogrammetric and Material Science Techniques in the Study of Materials on the Example of Alloy AlZnMgCu. Advances in Design, Simulation and Manufacturing II, 477–486)

Uhl, A. V., Melnyk, O. V., Melnyk, Y. A., Ilyin, L. V., 2021. Microphotogrammetric approach in the study of alsimg alloys. Metallofizika i Noveishie Tekhnologii 43(2).

Yasniy, P. V., Okipnyi, I. B., Maruschak, P. O., Bishchak, R. T., Sorochak, A. P., 2011. Toughness and failure of heat resistant steel before and after hydrogenation. Theoretical and Applied Fracture Mechanics, 56 (2), 63–67.